Modeling for Optimal Operation of PEM Fuel Cells and Electrolyzers

Paolo Gabrielli[1] and Ben Flamm[2], Annika Eichler[2], Matteo Gazzani[1], John Lygeros[2], Marco Mazzotti[1]
[1] Department of Mechanical Engineering, ETH Zürich, Separation Process Laboratory, Zürich, Switzerland
[2] Department of Electrical Engineering, ETH Zürich, Automatic Control Laboratory, Zürich, Switzerland
gapaolo@ipe.mavt.ethz.ch, flammb@control.ee.ethz.ch

***Abstract*—This contribution presents and analyzes modeling and minimum cost operation of proton exchange membrane (PEM) fuel cells and electrolyzers. First, detailed thermoelectric models of the electrochemical technologies based on a first-principle approach are presented. Then, as the detailed nonlinear models developed are intractable for use in online optimal control computation, a mixed integer linear program (MILP) is formulated with a piecewise affine approximation of the conversion efficiency and linear temperature dynamics for the devices. The outputs of the simplified linear models are compared with the detailed ones, when optimally producing and consuming a fixed quantity of hydrogen gas. Comparisons are performed for a variety of price scenarios and efficiency approximations, for both the fuel cell and electrolyzer.**

***Index Terms*—Hydrogen storage; Energy management; Fuel cells; Electrolyzers; Modeling; Optimization; Control.**

I. Introduction

Electric power markets are currently experiencing a significant transformation due to the increasing penetration of intermittent renewable energy sources (RES), and the shift from centralized to decentralized energy generation. In this context, hydrogen is a promising energy carrier because of its ability to bridge RES intermittency by storing energy, lose minimal energy when stored over long time periods, and produce carbon-free electricity when needed. However, improved energy conversion and storage devices are needed to enable the use of hydrogen as an energy carrier. This paper investigates the optimal operation of hydrogen-based conversion technologies. In particular, it considers an electrolyzer that converts water and electricity into hydrogen and oxygen, a product storage tank, and a fuel cell that recombines the two gases to generate electricity. The efficiency and thermal characteristics of the conversion devices depend on the chosen operating points. Therefore, to economically operate the underlying technologies for advanced electricity and gas grid interactions over long time horizons, computationally efficient and accurate models are needed.

This work consolidates and expands upon PEM modeling literature [1]-[7]. A theoretical and experimental static analysis of high pressure PEM electrolyzers is developed in [1], while a simple dynamic model for hydrogen output flow is proposed in [2]. Similarly, [4] and [5] develop a framework for the static and dynamic description of PEM fuel cells, while [6] and [7] present applications for distributed generation. This study incorporates the above works and adapts additional results for temperature dynamics in alkaline electrolyzers [8] and partial pressure dynamics in solid oxide fuel cells [9]. Also, the energy consumption of the auxiliary components, commonly referred to as the balance-of-plant (BoP), is accounted for. The resulting modeling framework consists of first-principle, thermoelectric models that allow for the prediction of the device dynamics, conversion performance and temperature levels.

This study also builds upon literature regarding the minimum cost operation of PEM electrolyzers and fuel cells. Previous papers investigated ways to optimally use power from wind turbines [11] and photovoltaics [12], considering time-varying electricity prices when deciding whether to supply power directly to the electricity grid or convert it to hydrogen gas for energy storage. Constant device conversion efficiency is assumed by [11], while [12] uses a nonlinear efficiency. A piecewise affine conversion efficiency approximation for a battery-based storage system is proposed by [13] for use in an optimization scheme with the goal of demand peak shaving. Unlike the above studies, the effect of various linear approximations of conversion efficiency and temperature constraints on the optimization problem are considered here.

This paper is structured as follows. In Section II, first-principle models of PEM devices are developed. In Section III, linear approximations of PEM device efficiency curves are introduced, followed by an optimization framework for evaluating these approximations. In Section IV, simulation results that verify and highlight various properties of the PEM device models are presented. Finally, the optimization results are checked against the detailed models and the influence of various linearization approximations are evaluated.

II. PEM Device Modeling

The electrolyzer and fuel cell are modeled with a first-principle, lumped approach, which accounts for electrochemical features and transport phenomena in the cell, including mass transport across the polymeric membrane as well as heat transfer. In the following, the main features of the thermodynamic models are described, while the entire set of equations describing the devices is summarized in Table I with the corresponding references. Similarly, the main assumptions made in the modeling framework are summarized in Table II.

978-1-5090-2320-2/16/$31.00

TABLE I
THERMODYNAMIC MODEL EQUATIONS.

	Electrolyzer		**Fuel cell**	
	Electrochemical model			
Cell voltage	$U = E + U_{\text{act}} + U_{\text{ohm}} + U_{\text{dif}}$	[1]	$U = E - U_{\text{act}} - U_{\text{ohm}} - U_{\text{dif}}$	[7]
Cell voltage - Nernst equation	$E = \frac{\Delta G^0(T)}{2F} - \frac{RT}{2F} ln \left(\frac{p_{\text{H}_2} \sqrt{p_{\text{O}_2}}}{p_{\text{H}_2\text{O}}} \right)$	[10]	$E = \psi_1 - \psi_2 T + \psi_3 T(\ln p_{\text{H}_2} + 1/2 \ln p_{\text{O}_2})$	[5]
Partial pressure dynamics	$p_j^{\text{o}} = \frac{n_j^g}{K_j} \left[1 - \exp\left(-\frac{t}{\tau_j} \right) \right]$		$p_j^{\text{o}} = \frac{n_j^{\text{i}} - n_j^{\text{con}}}{K_j} \left[1 - \exp\left(-\frac{t}{\tau_j} \right) \right]$	[6], [9]
Activation term	$U_{\text{act}} = \frac{RT}{\zeta F} \operatorname{arcsinh}\left(\frac{i}{zi^0} \right)$	[1]	$U_{\text{act}} = \phi_1 + \phi_2 T + \phi_3 T \ln(i)$	[5]
Ohmic term	$U_{\text{ohm}} = (R_e + R_m) I$	[2]	$U_{\text{ohm}} = (R_e + R_m) I$	[5]
Concentration term	$U_{\text{dif}} = \frac{RT}{zF} \ln \left(\frac{q_{i,m}}{q_{i,m}^0} \right)$	[1]	$U_{\text{dif}} = -B \ln \left(1 - \frac{I}{I_{\max} A_{\text{cell}}} \right)$	[5]
	Mass balances			
Water balance - anode	$n_{\text{H}_2\text{O}}^{\text{an,o}} = n_{\text{H}_2\text{O}}^{\text{an,i}} - n_{\text{H}_2\text{O}}^{\text{con}} - n_{\text{H}_2\text{O}}^{\text{dif}} - n_{\text{H}_2\text{O}}^{\text{eod}}$	[1]	$n_{\text{H}_2\text{O}}^{\text{an,o}} = n_{\text{H}_2\text{O}}^{\text{an,i}} + n_{\text{H}_2\text{O}}^{\text{g}}$	
Water balance - cathode	$n_{\text{H}_2\text{O}}^{\text{cat,o}} = n_{\text{H}_2\text{O}}^{\text{dif}} + n_{\text{H}_2\text{O}}^{\text{eod}}$	[1]	-	
Hydrogen balance - anode	$n_{\text{H}_2}^{\text{an,o}} = n_{\text{H}_2}^{\text{dif}}$	[3]	$n_{\text{H}_2}^{\text{an,o}} = n_{\text{H}_2}^{\text{an,i}} - n_{\text{H}_2}^{\text{con}}$	
Hydrogen balance - cathode	$n_{\text{H}_2}^{\text{cat,o}} = \left(n_{\text{H}_2}^{\text{g}} - n_{\text{H}_2}^{\text{dif}} \right) \left[1 - \exp\left(-\frac{t}{\sigma_{\text{H}_2}} \right) \right]$	[2], [3]	-	
Oxygen balance - anode	$n_{\text{O}_2}^{\text{an,o}} = n_{\text{O}_2}^{\text{g}} \left[1 - \exp\left(-\frac{t}{\sigma_{\text{O}_2}} \right) \right]$		-	
Oxygen balance - cathode	-		$n_{\text{O}_2}^{\text{an,o}} = n_{\text{O}_2}^{\text{an,i}} - n_{\text{O}_2}^{\text{con}}$	
Water consumed/generated	$n_{\text{H}_2\text{O}}^{\text{con}} = \eta_F \frac{NI}{2F}$	[3]	$n_{\text{H}_2\text{O}}^{\text{g}} = \frac{NI}{2F}$	[7]
Hydrogen generated/consumed	$n_{\text{H}_2}^{\text{g}} = \eta_F \frac{NI}{2F}$	[3]	$n_{\text{H}_2}^{\text{con}} = \frac{NI}{2F}$	[7]
Oxygen generated/consumed	$n_{\text{O}_2}^{\text{g}} = \eta_F \frac{NI}{4F}$	[3]	$n_{\text{O}_2}^{\text{con}} = \frac{NI}{4F}$	[7]
Inlet water/hydrogen	$n_{\text{H}_2\text{O}}^{\text{i}} = \eta_F \frac{NI}{2Fu}$		$n_{\text{H}_2}^{\text{i}} = \frac{NI}{2Fu}$	
	Thermal model			
Energy balance	$C_{\text{t}} \frac{\text{d}T}{\text{d}t} = Q_{\text{g}} - Q_{\text{l}} - Q_{\text{c}}$	[2], [8]	$C_{\text{t}} \frac{\text{d}T}{\text{d}t} = Q_{\text{g}} - Q_{\text{l}} - Q_{\text{c}}$	
Generated heat	$Q_{\text{g}} = NI(U - U_{\text{tn}}) = NIU(1 - \eta_{\text{U}})$	[2], [8]	$Q_{\text{g}} = NI(U_{\text{tn}} - U) = NIU(\frac{1}{\eta_{\text{U}}} - 1)$	
Lost heat	$Q_{\text{l}} = \frac{T - T_{\text{a}}}{R_{\text{t}}}$	[2], [8]	$Q_{\text{l}} = \frac{T - T_{\text{a}}}{R_{\text{t}}}$	
Cooling heat	$Q_{\text{c}} = m_{\text{c}} c_{\text{c}} (T_{\text{c}}^{\text{i}} - T_{\text{c}}^{\text{o}}) = H_{\text{hx}} \text{LMTD}$	[8]	$Q_{\text{c}} = m_{\text{c}} c_{\text{c}} (T_{\text{c}}^{\text{i}} - T_{\text{c}}^{\text{o}}) = H_{\text{hx}} \text{LMTD}$	
	Balance of plant			
Balance of plant power	$P_{\text{BOP}} = \left(\frac{v_{\text{H}_2\text{O}} \Delta p}{\eta_{\text{P}}} \right) + P \left(\frac{1}{\eta_{\text{C}}} - 1 \right) + \gamma$		$P_{\text{BOP}} = P \left(\frac{1}{\eta_{\text{C}}} - 1 \right) + \gamma$	

For sake of clarity, nomenclature is reported at the end of the paper in Table IV.

A. PEM Electrolyzer

A high pressure PEM electrolyzer (EC) is modeled. When electric current is run through deionized water, hydrogen and oxygen are produced at a pressure of 40 bar.

Electrochemical Model. The cell voltage U is the sum of the open-circuit voltage E and a series of overvoltages, namely the activation, ohmic, and diffusion overvoltages.

The open-circuit voltage is evaluated using the Nernst equation, where the partial pressure dynamics are modeled after the approach originally introduced in [9] for solid oxide fuel cells (SOFCs). The partial pressures of the gas products p are related to the corresponding molar flow rate n by a first order transfer function. Taking hydrogen as an example

$$p_{\text{H}_2} = \frac{n_{\text{H}_2}^{\text{g}}}{K_{\text{H}_2}} \left[1 - \exp\left(-\frac{t}{\tau_{\text{H}_2}} \right) \right]$$

where $n_{\text{H}_2}^{\text{g}}$ is the generated hydrogen, K_{H_2} the hydrogen valve constant, $\tau_{\text{H}_2} = V_{\text{cat}}/(K_{\text{H}_2} RT)$ the time constant associated with the hydrogen flow, and V_{cat} the cathode volume. The product output flows are also characterized by first order linear dynamics [2].

The overpotentials have the effect of increasing the actual cell voltage. For the same absorbed power, this implies a decrease in the cell current I and thus in the hydrogen production. The activation overvoltage expresses the charge transfer limitations occurring at the electrode/electrolyte interface. This is also called the activation energy for the electrode reaction. This contribution is predominant at low current densities and can be expressed through the Butler-Volmer equation for each electrode [1], [10]. Moreover, the ohmic overvoltage quantifies the ohmic resistances across the components of the stack and is predominant at medium current densities. Here, a lumped electronic resistance across the electrodes and ionic resistance (typically predominant) across the polymeric membrane are

included as in [2]. Finally, the diffusion (or concentration) overvoltage accounts for mass transport limitations, and is predominant at high current densities. For water electrolysis, the main contribution to the diffusion overvoltage is given by the transport of the product gases, modeled as in [1].

Mass Balance. The water balance includes the water flowing from the anode to the cathode due to concentration gradient and electro-osmotic drag. No pressure gradient is present across the polymeric membrane as both anode and cathode are simulated at $40\,\mathrm{bar}$. These transport phenomena are modeled as in [1]. The hydrogen balance accounts for the hydrogen permeating from the cathode to the anode due to the concentration gradient, defined as in [3]. Finally, the generated hydrogen and oxygen, as well as the consumed water, are determined by Faraday's law. A Faraday efficiency η_F of 0.99 is used [3], and a utilization factor u varying with power is considered.

Thermal Model. The thermal behavior of the electrolyzer is described through a lumped thermal capacitance, C_t. The energy balance includes the generated heat Q_g, the heat lost to the environment Q_l, and the heat removed by the cooling system Q_c [2], [8]:

$$C_\mathrm{t}\frac{\mathrm{d}T}{\mathrm{d}t} = Q_\mathrm{g} - Q_\mathrm{l} - Q_\mathrm{c} \tag{1}$$

$$Q_\mathrm{g} = NI(U - U_\mathrm{tn}) = NIU(1-\eta_\mathrm{U}) \tag{2}$$

$$Q_\mathrm{l} = \frac{T - T_\mathrm{a}}{R_\mathrm{t}} \tag{3}$$

TABLE II
PEM MODEL PARAMETERS.

Paremeter	Unit	Electrolyzer	Fuel cell
A_cell	cm^2	170	180
C_t	kJ/°C	250	350
C_{p_c}	kJ/(kg °C)	4.18	4.18
$H_\mathrm{hx}A_\mathrm{hx}$	W/°C	380	500
K_{H_2}	mol/(bar s)	5.18E-03	4.17E-02
$K_{\mathrm{H}_2\mathrm{O}}$	mol/(bar s)	-	7.62E-03
K_{O_2}	mol/(bar s)	3.17E-03	2.08E-02
m_c	kg/s	0.25	0.25
N		200	400
P_max	kW	100	100
p_des	bar	40	3
R_t	°C/mol	0.082	0.082
T_0	°C	25	25
T_a	°C	25	25
T_c^i	°C	20	20
T_des	°C	70	70
T_max	°C	80	80
u		0.85 - 0.99	0.85 - 0.99
V^S	m^3	5	5
γ	W	2500	360
σ_{H_2}	s	4	-
σ_{O_2}	s	6	-
τ_{H_2}	s	2.07	3.37
$\tau_{\mathrm{H}_2\mathrm{O}}$	s	-	18.4
τ_{O_2}	s	4.14	6.74

$$Q_\mathrm{c} = m_\mathrm{c}c_{p_\mathrm{c}}(T_\mathrm{c}^\mathrm{i} - T_\mathrm{c}^\mathrm{o}) = A_\mathrm{hx}H_\mathrm{hx}\mathrm{LMTD} \tag{4}$$

where N is the number of cells, $U_\mathrm{tn} = \Delta H^0/(2F)$ the thermoneutral voltage, and $\eta_\mathrm{U} = U_\mathrm{tn}/U$ the voltage efficiency, quantifying the percentage of voltage used for gas generation (rather than lost as heat); T is the device temperature, T_a the ambient temperature, and R_t the lumped thermal resistance; m_c is the coolant mass flow rate, c_{p_c} is the coolant specific heat at constant pressure, T_c^i the coolant inlet temperature, T_c^o the coolant outlet temperature, A_hx the heat exchanger area, H_hx the overall heat transfer coefficient of the heat exchanger, and LMTD the logarithmic mean temperature difference between T_c^i and T_c^o. For the purpose of modeling, the parameters above are chosen based on values reported in [2] and [8], and reported in table II.

Rearranging (1)-(4) leads to the differential equation

$$\frac{\mathrm{d}T}{\mathrm{d}t} = -\alpha T + \beta. \tag{5}$$

$$\alpha = \frac{1}{\tau_\mathrm{t}} + \frac{C_\mathrm{c}}{C_\mathrm{t}}\left[1 - \exp\left(\frac{-A_\mathrm{hx}H_\mathrm{hx}}{C_\mathrm{c}}\right)\right] \tag{6}$$

$$\beta = \frac{NIU(1-\eta_\mathrm{U})}{C_\mathrm{t}} + \frac{T_\mathrm{a}}{\tau_\mathrm{t}} + \frac{C_\mathrm{c}T_\mathrm{c}^\mathrm{i}}{C_\mathrm{t}}\left[1 - \exp\left(\frac{-A_\mathrm{hx}H_\mathrm{hx}}{C_\mathrm{c}}\right)\right] \tag{7}$$

The quantity $\tau_\mathrm{t} = R_\mathrm{t}C_\mathrm{t}$ represents the thermal time constant, and $C_\mathrm{c} = m_\mathrm{c}c_{p_\mathrm{c}}$ is the thermal capacity of the liquid water coolant.

Auxiliary Electrical Components. The electrolyzer model includes an AC/DC converter, a water pump, and a gas cleaning system as part of the BoP. The converter is modeled as a constant efficiency η_c between the power provided by the electrical grid and absorbed by the electrolyzer. The pump is modeled as an additional source of power consumption, proportional to the inlet water volume flow $v_{\mathrm{H}_2\mathrm{O}}$ and the pump pressure difference Δp. On the other hand, a constant power γ is drawn by the gas cleaning system and additional auxiliary devices such as controllers and sensors.

B. PEM Fuel Cell

The approach described for the electrolyzer is similarly implemented to simulate the PEM fuel cell (FC). The main difference lays in the electrochemical model, where correlations from [5] are implemented to simulate the open circuit voltage and the voltage losses, and in the mass balances. The complete model, based on [4]-[10] is summarized in Table I. Electricity is generated by using hydrogen and oxygen as fuel and oxidant, respectively, both at $3\,\mathrm{bar}$. In this case, the voltage inefficiencies decrease the cell voltage, increasing the consumed hydrogen. A DC/AC converter is included in the variable BoP.

C. Storage

The storage facilities (S) are simulated as pressurized vessels storing gaseous hydrogen and oxygen at $25\,^\circ\mathrm{C}$ and $40\,\mathrm{bar}$.

III. Optimization Framework for Linear Approximation Methods

Hydrogen energy storage, coupled with an electrolyzer and fuel cell, allows for novel interactions with the electricity and gas grids. These interactions could include providing reserve services to the grid, performing arbitrage in the presence of fluctuating spot market prices, and exploring the interplay between electricity grids and personal mobility. For these scenarios, optimal control problems can be formulated to optimize a utility function, subject to the device constraints. Unfortunately, due to the underlying nonlinear behavior of PEM fuel cells and electrolyzers, it is intrinsically difficult to develop an optimization framework using detailed models.

A. System Efficiency Approximation

Here, linear and piecewise affine (PWA) approximations of the relationship between device power P and input/output gas volume $V(P)$ are developed. Note that the gas volume produced or consumed also depends on the device temperature. However, the temperature dependence is neglected here, as discussed in detail below. Additionally, hereafter only hydrogen is considered, as oxygen is assumed to be produced or consumed in a 2:1 $H_2 : O_2$ stoichiometric ratio. Finally, only the electrolyzer is treated here; similar results hold for the FC as explained below.

The detailed PEM electrolyzer model developed in Section II can be used to generate a discretized efficiency curve consisting of K points $\{(P_{\text{in}}^{(1)},\dots,P_{\text{in}}^{(K)}),(V_{\text{out}}^{(1)},\dots,V_{\text{out}}^{(K)})\}$. The following methods to approximate this discretized curve are depicted in Fig. 1.

1) Linear Efficiency Approximation: The linear approximation of the device input-to-output efficiency curve is taken as the best-fit line which goes through the origin, since zero input power should result in zero output gas.

2) PWA Efficiency Approximation: The PWA approximation of the detailed efficiency curve is generated by choosing the optimal position of n breakpoints $\{(b_{\text{in}}^{(1)},\dots,b_{\text{in}}^{(n)}),(b_{\text{out}}^{(1)},\dots,b_{\text{out}}^{(n)})\}$ to solve the following optimization problem:

$$\underset{b_{\text{in}}^{(1)},\dots,b_{\text{in}}^{(n)}}{\text{minimize}} \sum_{k=1}^{K}\left(b_{\text{out}}^{(j)}+m^{(j+1)}(P_{\text{in}}^{(k)}-b_{\text{in}}^{(j)})-V_{\text{out}}^{(k)}\right)^2 \quad (8)$$

with j the largest index such that $P_{\text{in}}^{(k)} \geq b_{\text{in}}^{(j)}$, subject to the following constraints for all $i \in [1,n]$:

$$m^{(i)} = \frac{b_{\text{out}}^{(i)}-b_{\text{out}}^{(i-1)}}{b_{\text{in}}^{(i)}-b_{\text{in}}^{(i-1)}}$$
$$m^{(i)} \geq m^{(i+1)} \quad (9)$$
$$m^{(n+1)}$$
$$= \underset{m}{\text{argmin}} \sum_{j:P_{\text{in}}^{(j)}\geq b_{\text{in}}^{(n)}}\left(b_{\text{out}}^{(n)}+m(P_{\text{in}}^{(j)}-b_{\text{in}}^{(n)})-V_{\text{out}}^{(j)}\right)^2 \quad (10)$$
$$b_{\text{in}}^{(0)} = b_{\text{out}}^{(0)} = 0$$
$$b_{\text{in}}^{(1)} \leq \dots \leq b_{\text{in}}^{(n)}$$
$$b_{\text{out}}^{(i)} = V_{\text{out}}^{(l)} + \frac{V_{\text{out}}^{(l+1)}-V_{\text{out}}^{(l)}}{P_{\text{in}}^{(l+1)}-P_{\text{in}}^{(l)}}\left(b_{\text{in}}^{(i)}-P_{\text{in}}^{(l)}\right) \quad (11)$$

with l the largest index such that $P_{\text{in}}^{(l)} \leq b_{\text{in}}^{(i)}$.

In other words, the PWA approximation consists of $n+1$ line segments with corresponding slopes $m^{(1)},\dots,m^{(n+1)}$ constrained by (9) to preserve the convexity of the optimization control problem discussed below. Slope $m^{(n+1)}$ is equal to the best-fit slope of the set of discretized efficiency curve points $\{(P_{in}^{(j)},V_{out}^{(j)})\}$, for all j such that $P_{in}^{(j)} \geq b_{\text{in}}^{(n)}$ (10). The breakpoints are chosen to minimize the mean square error (8), and are restricted to lie on the linear interpolants of the discretized efficiency curve (11).

As this fitting problem is nonlinear, it is solved in Matlab using fmincon. The solution routine uses an initial guess of the breakpoints consisting of n uniformly-spaced points between 0 and $P_{\text{in}}^{(K)}$. Note that the fitting problem can be precomputed for a given device efficiency curve, and hence is not time-critical.

The volume generated at input power P is specified as

$$V(P) = b_{\text{out}}^{(j)} + m^{(j+1)}\left(P-b_{\text{in}}^{(j)}\right)$$

where, as above, j is the largest index with $P \geq b_{\text{in}}^{(j)}$. Due to the concavity of the piecewise approximation

$$V(P) = \underset{i\in\{1,\dots,n\}}{\text{minimum}}\left(b_{\text{out}}^{(i)}+m^{(i+1)}\left(P-b_{\text{in}}^{(i)}\right)\right). \quad (12)$$

Similar treatment holds for the FC. In this case, the volume input to power output curve is considered, the PWA approximation of which must also be monotone non-increasing.

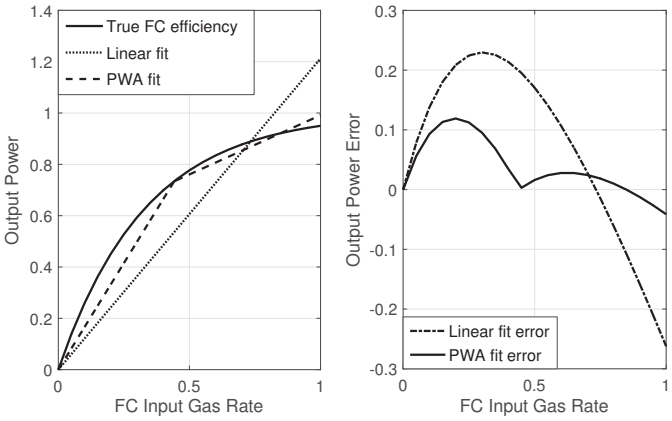

Fig. 1. (L) Methods used to approximate PEM fuel cell conversion efficiency. Data is normalized, not representative. (R) Error due to various approximation schemes. Note that breakpoint of PWA fit has zero error.

B. Optimal Operation Strategy

A mixed integer linear program (MILP) is formulated to determine the minimum-cost control strategy for the PEM devices. The formulation for the electrolyzer seeks to produce

a desired amount of hydrogen at minimum cost over a day-long horizon with 15 minute timesteps, optimizing over the power input $P \in \mathbb{R}^N$ and the binary state $\delta \in \{0,1\}^N$. The binary state specifies whether the device is turned on, producing power but also incurring the BoP cost. The electricity price as a function of the time of the day p is given, as well as the system thermal parameters and the constant term in the BoP, γ, reported in table II. The coolant mass flow is kept constant during operation. The initial temperature is specified by T_0, and the final volume defined by V_N^S. The optimization problem is formulated as

$$\underset{P,\delta}{\text{minimize}} \sum_{t=1}^{N} p[t](P[t] + \gamma\delta[t])$$

subject to

$$V^{\mathrm{S}}[t+1] = V^{\mathrm{S}}[t] + V(P[t]) \tag{13}$$

$$T[t+1] = \alpha T[t] + \beta' \tag{14}$$

$$T[t] \leq T_{\max}$$

$$0 \leq P[t] \leq P_{\max}\delta[t]$$

$$V^{\mathrm{S}}[t] \geq 0, V^{\mathrm{S}}[0] = 0, V^{\mathrm{S}}[N] = V_N^{\mathrm{S}}, T[0] = T_0$$

for $t \in [1, \ldots, N]$, where $N = 96$ is the number of timesteps. In (13), $V(P[t])$ is computed using an approximation of the detailed efficiency curves as in (12).

In (14), the continuous time temperature progression (5) is discretized and linearized. A Forward Euler (First-Order Hold) method is used to discretize and integrate the discrete time dynamics. Although the voltage efficiency η_{U} in β generally depends on temperature and power in (7), it is assumed constant in β', thus linearizing the temperature dynamics in the MILP. Here, $\eta_{\mathrm{U}} = 0.7$ is selected for both the electrolyzer and the fuel cell, as a tradeoff between a conservative lower value that assumes that more of the cell voltage is transformed into heat, and a higher value that allows the electrolyzer to work closer to the temperature limit, where it has higher efficiency.

The fuel cell optimization problem proceeds similarly and independently. It seeks to maximize the revenue of the net generated electricity while using a fixed quantity of hydrogen. The temperature state progression, and power, temperature, and volume constraints are similar to those of the electrolyzer.

IV. Results and Discussion

A. PEM Modeling and Linearization Results

This work considers a 100 kW PEM electrolyzer and fuel cell. Fig. 2 shows the hydrogen production of the electrolyzer (a) and the hydrogen consumption of the fuel cell (b) versus the input or output power for various operating temperatures. The time response of hydrogen production (c) and cell temperature (d) are also depicted for a step variation in the electrolyzer absorbed power from 0 to 100 kW. The hydrogen flow exhibits a fast dynamic response on the order of seconds, while the temperature dynamics responds on the order of minutes. This validates the decision to consider only

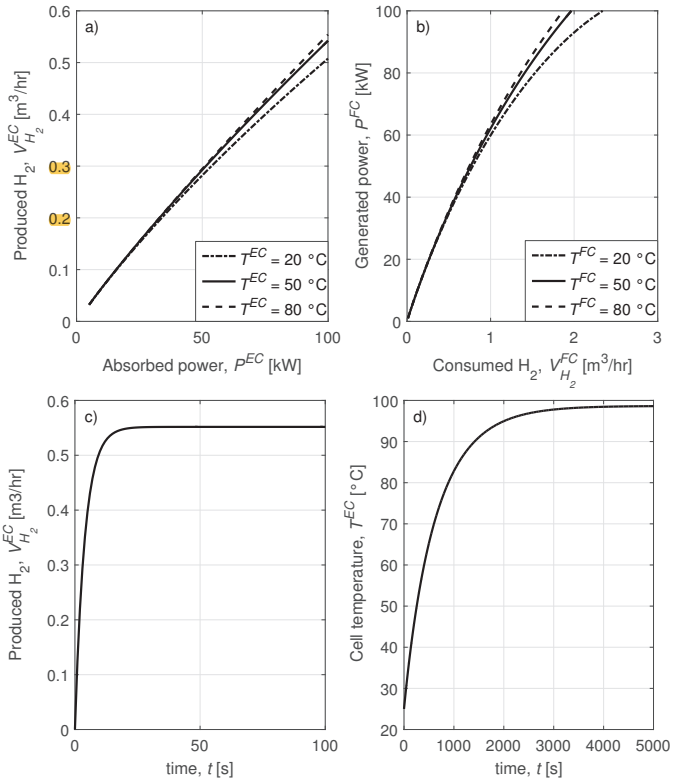

Fig. 2. Conversion efficiency for the electrolyzer (a) and the fuel cell (b) for T = 20, 50, 80 °C; Electrolyzer response of hydrogen production (c) and cell temperature (d) for a 0 to 100 kW step in absorbed power.

temperature dynamics in the 15-minute resolution optimization problem. Note that in practice, the temperature progression in (14) is integrated over a 1-minute period to improve accuracy.

In addition to the performance curve linearization, another source of error is present in the temperature dynamics (14), linearized by neglecting the temperature and power dependencies of η_U in β'. This approximation error is illustrated for the fuel cell in Fig. 3.

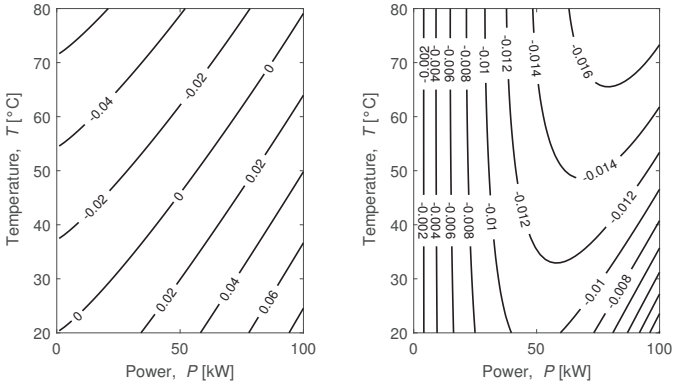

Fig. 3. (L) Simulated FC temperature change rate in °C/s with respect to power and temperature. (R) Absolute error [°C/s] when linearizing temperature change rate as done in MILP, assuming constant voltage efficiency.

B. Optimization Results

Next, several linear and PWA efficiency approximations are considered for use in the MILP optimal control scheme, and the resulting performance is analyzed. For each approximation, the MILP is solved for the optimal daily electrolyzer production or FC consumption of five cubic meters of hydrogen, with the price known in advance for the entire optimization horizon. The computed optimal power profile is then simulated in the detailed model, and the resulting volume and temperature state progressions are compared to the simplified MILP results. Fig. 4 shows the optimal consumed/produced electrical power resulting from the optimization for a typical Swiss summer spot market price [14] and a PWA approximation with one breakpoint.

Table III summarizes the simulation outcomes for a typical Swiss spot market price in summer [14] and a low-high price profile based on Zurich time-of-day rates [15]. The following indicators are used to compare detailed and approximate models. The temperature violation Θ expresses the time integral of the temperature constraint ($80\,^{\circ}\mathrm{C}$) violation. Hydrogen volume discrepancies are reported for two different detailed simulations: (i) Γ, for a constant coolant flow rate and corresponding temperature evolution; (ii) Λ, for a constant operating temperature (as if an independent coolant flow rate controller were present). Since the latter simulation runs at a constant temperature, it removes the effect of temperature dependency, and highlights the effect of the efficiency linearization. A positive hydrogen volume error for the FC means too much gas has been consumed, while a negative error for the electrolyzer means too little gas has been produced. The cost suboptimality Ω indicates the cost that could be saved by switching to a policy found by using a PWA approximation with a large number of breakpoints n (30 in this case). This additional cost is calculated by using the actual volume consumption/production given by the detailed models. Note that a 30-breakpoint approximation would include considerably more constraints, rendering the problem harder to compute. Also, since the approximate volume consumption/production neglects the temperature dependency and linearizes the temperature dynamics, a lower cost outcome might exist using the exact nonlinear model.

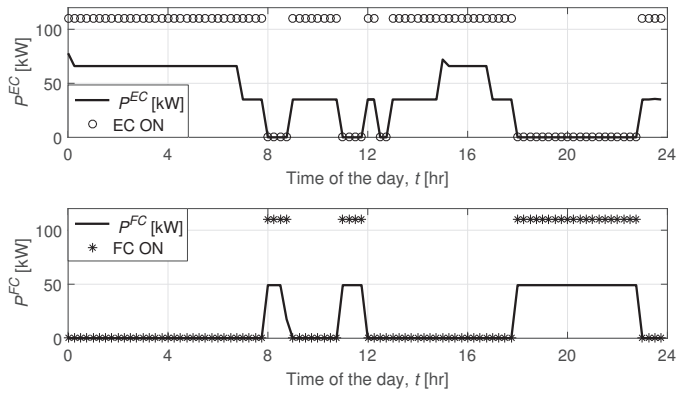

Fig. 4. Optimization results for a typical Swiss spot market price in summer [14] and PWA approximation with $n = 1$: EC consumed electrical power (above) and FC produced electrical power (below).

TABLE III
COMPARISON BETWEEN DETAILED AND APPROXIMATE MODELS FOR TEMPERATURE VIOLATION (Θ), H_2 VOLUME ERROR (Γ), H_2 VOLUME ERROR WITH CONSTANT DEVICE TEMPERATURE (Λ), AND COST SUBOPTIMALITY (Ω).

	Price scenario: Electricity spot market - Summer			
	Θ [°C min/day]	Γ	Λ	Ω
FC - Linear	1820	2.84%	2.95%	-18.4%
FC - PWA, $n = 1$	0	0.46%	-0.19%	-7.02%
FC - PWA, $n = 2$	0	0.49%	-0.09%	-2.62%
FC - PWA, $n = 30$	0	0.33%	-0.01%	-
EC - Linear	0	-0.37%	0.62%	2.13%
EC - PWA, $n = 1$	0	0.03%	0.50%	1.16%
EC - PWA, $n = 2$	0	-0.16%	0.22%	0.71%
EC - PWA, $n = 30$	0	-0.45%	-0.01%	-
	Price scenario: Low-high price			
	Θ [°C min/day]	Γ	Λ	Ω
FC - Linear	155	13.0%	10.29%	-31.1%
FC - PWA, $n = 1$	0	1.18%	-0.23%	-10.9%
FC - PWA, $n = 2$	0	0.62%	-0.09%	-4.25%
FC - PWA, $n = 30$	0	0.34%	-0.01%	-
EC - Linear	0	-1.02%	-0.47%	2.70%
EC - PWA, $n = 1$	0	-0.12%	0.45%	1.18%
EC - PWA, $n = 2$	0	-0.29%	0.21%	1.21%
EC - PWA, $n = 30$	0	-0.58%	-0.01%	-

A few salient results emerge from the simulations: (i) in most cases, the linearization of the conversion efficiency leads to an underestimation of the produced hydrogen and an overestimation of the consumed hydrogen. This is due to the curve-fitting algorithm, which ensures that operating at power levels between breakpoints will result in estimates on one side of the actual efficiency curve, depending on the curve concavity. (ii) Depending on the relative magnitudes of the effects of the temperature and power on the device efficiency, increasing the number of breakpoints does not necessarily lead to a more accurate system approximation. Indeed, a larger number of breakpoints can lead to lower-power operating points, where the conversion efficiency is higher. However, in these conditions a device is run at a temperature lower than the reference value for the given efficiency curve, resulting in a lower EC gas production and a greater FC gas consumption, and increasing the discrepancy relative to the detailed models. (iii) Although the limiting case of 30 breakpoints is not necessarily the best approximation of system temperature and volume production/consumption, it does minimize total cost. (iv) Constant efficiency approximations perform uniformly worse than the PWA efficiency approximations, in terms of temperature violations, volume error, and cost. (v) The PWA fit appears to be a reasonable approximation of the underlying models, especially if operating the PEM devices under

TABLE IV
NOMENCLATURE.

Thermodynamic models			
Symbols		η_C	AC/DC converter efficiency
C	thermal capacity, [W/°C]	η_F	Faraday efficiency
c_p	specific heat, [J/(kg°C)]	η_P	pump efficiency
E	open circuit voltage, [V]	η_U	voltage efficiency
F	Faraday's constant, [°C/mol]	σ, τ	time constant, [s]
H	heat transfer coefficient [W/(°C m^2)]	ϕ	fitting coefficient
I	current, [A]	ψ	fitting coefficient
i	current density, [A/m^2]	*Subscripts*	
K	valve constant, [mol/(atm s)]	a	ambient
m	mass flow rate, [kg/s]	act	activation
N	number of stack cells	BOP	balance-of-plant
n	molar flow rate, [mol/s]	c	cooling
P	electrical power, [W]	cell	cell of the stack
p	pressure, [Pa]	des	design conditions
Q	thermal power, [W]	dif	diffusion
q	molar concentration, [mol/m^3]	hx	heat exchanger
R	ideal gas constant, [J/(mol K)]	j	j-th component
R_e	electronic resistance, [Ω]	l	natural losses
R_m	ionic resistance, [Ω]	m	membrane
T	temperature, °C	max	maximum limit
t	time variable, [s]	t	thermal
V	volume, [m^3]	*Superscripts*	
v	volume flow rate, [m^3/s]	0	reference condition
U	cell voltage, [V]	an	anode
U_{tn}	thermo-neutral voltage, [V]	cat	cathode
Greek letters		con	consumed
α	temperature evolution constant, [1/s]	eod	electro-osmotic drag
β	temperature evolution constant, [°C/s]	g	generated
γ	power-independent BOP, [W]	i	inlet section
ζ	charge transfer coefficient	o	outlet section
Optimization framework			
Symbols		t	discrete time variable, [s]
b	breakpoint position	*Greek letters*	
i, j	generic breakpoint	Γ	volume error, [%]
K	number of discretization points	δ	binary variable for ON/OFF operation
k	generic discretization point	Λ	volume error, [%]
m	linear interpolant slope	Θ	temperature violation, [°C min/day]
N	number of timesteps	Ω	cost suboptimality, [%]
n	number of breakpoints	*Superscripts*	
p	electricity price, [EUR/kWh]	S	storage

constant temperature control. Additionally, unlike nonlinear models, PWA approximations are better suited to an online optimization framework.

An additional remark is merited about PWA breakpoint placement on the linear interpolants of the discretized efficiency curve. MILP optimization problems return solutions at constraint vertices. Since the breakpoints serve as constraint vertices, the linear program will choose one of these vertices as a solution unless another constraint (such as volume or temperature) is active. If the operating point is on the interpolant of the efficiency curve, this is the most accurate efficiency value.

V. CONCLUSION

This paper uses first-principle models to analyze approximations made in the optimal control of a PEM electrolyzer and fuel cell. The models accurately reproduce the main conversion performance and dynamic features of the devices. Several efficiently-computable linear approximations are used to calculate the optimal daily production or consumption of five cubic meters of hydrogen at 40 bar, for typical price scenarios. The results of the optimization are then checked against the detailed models to determine the temperature and hydrogen volume modeling errors.

The PWA fitting of the efficiency curves, with one and two breakpoints, slightly increases the complexity of the problem relative to the linear approximation, as it introduces additional constraints into the MILP used to compute the optimal device inputs. While the computational time is not appreciably affected, the model accuracy is significantly improved, and the minimum operation cost reduced. Sources of error in the MILP include the nonlinear dependency of conversion performance and temperature dynamics on device power level, the temperature dependency of the system efficiency (particularly for the fuel cell), and the discretization of the temperature evolution.

ACKNOWLEDGMENT

The work was supported by the National Research Program "Energy Turnaround" (NRP70) of the Swiss National Science Foundation (SNSF), as well as the Alstom and ETH Zurich Foundation seed project "Behavioural and Technical Optimisation for Building Energy Efficiency and Flexibility."

REFERENCES

[1] F. Marangio, M. Santarelli, and M. Calì, "Theoretical model and experimental analysis of a high pressure PEM water electrolyser for hydrogen production", Int. J. Hydrogen Energy, vol. 34, no. 3, pp. 1143-1158, 2009.
[2] R. García-Valverde, N. Espinosa, and A. Urbina, "Simple PEM water electrolyser model and experimental validation", Int. J. Hydrogen Energy, vol. 37, pp. 1927-1938, 2012.
[3] H. Kim, M. Park, and K. S. Lee, "One-dimensional dynamic modeling of a high-pressure water electrolysis system for hydrogen production", Int. J. Hydrogen Energy, vol. 38, pp. 2596-2609, 2013.
[4] J. C. Amphlett, R. F. Mann, B. A. Peppley, P. R. Roberge, and A. Rodrigues, "A model predicting transient response of proton exchange membrane fuel cells", J. Power Sources, vol. 61, pp. 183-188, 1996.
[5] R. F. Mann, J. C. Amphlett, M. A. I. Hooper, H. M. Jensen, B. A. Peppley, and P. R. Roberge, "Development and application of a generalised steady-state electrochemical model for a PEM fuel cell", J. Power Sources, vol. 86, no. 1-2, pp. 173-180, 2000.
[6] El-Sharkh MY, Rahman A, Alam MS, Byrne PC, Sakla AA, Thomas T. A dynamic model for a stand-alone PEM fuel cell power plant for residential applications. J. Power Sources, vol. 138, pp. 199–204, 2004.
[7] M. H. Nehrir and C. Wang, "Modeling and Control of Fuel Cells: Distributed Generation Applications", 2009.
[8] Ulleberg Ø. "Modeling of advanced alkaline electrolyzers:a system simulation approach." Int. J. Hydrogen Energy 2003; 28:21e33.
[9] J. Padullés, G. . Ault, and J. McDonald, "An integrated SOFC plant dynamic model for power systems simulation", J. Power Sources, vol. 86, no. 1-2, pp. 495-500, 2000.
[10] Prentice G. "Electrochemical engineering principles". Prentice-Hall International Editions, 1991.
[11] Korpaas, M., Holen, A. T., and Hildrum, R. "Operation and sizing of energy storage for wind power plants in a market system." International Journal of Electrical Power & Energy Systems, 25(8), 599–606, 2003.
[12] P.L. Zervas, H. Sarimveis, J.A. Palyvos, N.C.G. Markatos, "Model-based optimal control of a hybrid power generation system consisting of photovoltaic arrays and fuel cells", Journal of Power Sources, vol. 181, Issue 2, pp 327-338, 2008.
[13] Koller, M., Borsche, T., Ulbig, A., and Andersson, G. "Review of grid applications with the Zurich 1MW battery energy storage system." Electric Power Systems Research, 120(March), 128–135, 2015.
[14] Swiss Spot Market Price, Dec 1, 2014. https://www.epexspot.com/en.
[15] EWZ Stromtarif 2016, ewz.basis. https://www.ewz.ch/content/dam/ewz/services/dokumentencenter/energie-beziehen/dokumente/gruener-strom-fuer-mein-zuhause/stromtarif-2016-zh-private.pdf.